IEEE Photonics Journal
An IEEE Photonics Society Publication

Open Access

High Spatially Resolved Idler Image With a Compact Noncollinear Optical Parametric Amplifier Using a CW Laser as Signal

Volume 7, Number 6, December 2015

Xuanke Zeng
Yi Cai
Wenting Chen
Shuiqin Zheng
Jingzhen Li
Tianlong Zhu
Shixiang Xu

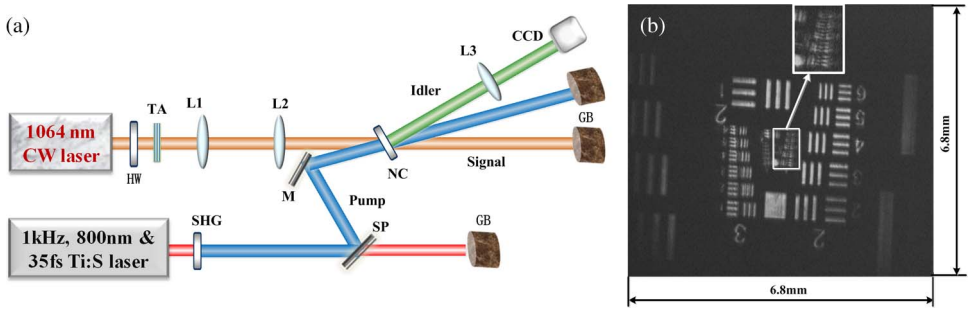

DOI: 10.1109/JPHOT.2015.2502785
1943-0655 © 2015 IEEE

IEEE photonics SOCIETY

IEEE

High Spatially Resolved Idler Image With a Compact Noncollinear Optical Parametric Amplifier Using a CW Laser as Signal

Xuanke Zeng, Yi Cai, Wenting Chen, Shuiqin Zheng, Jingzhen Li, Tianlong Zhu, and Shixiang Xu

Shenzhen Key Laboratory of Micro-Nano Photonic Information Technology, College of Electronic Science and Technology, Shenzhen University, Shenzhen 518060, China

DOI: 10.1109/JPHOT.2015.2502785

Manuscript received October 13, 2015; revised November 16, 2015; accepted November 18, 2015. Date of publication November 23, 2015; date of current version December 3, 2015. This work was supported in part by the National Natural Science Funds of China under Grant 61275101, Grant 6140119, and Grant 61027014 and in part by the Specialized Research Fund for the Shenzhen Strategic Emerging Industries Development under Grant JCYJ20140418181958481 and Grant JCYJ20150525092941064. Corresponding author: S. Xu (e-mail: shxxu@szu.edu.cn).

Abstract: We realize a high spatially resolved idler imaging with a compact noncollinear optical parametric amplifier, which is based on type-II phase matching (PM). Using an intense femtosecond laser pulse train as the pump, this amplifier can amplify a separate continuous-wave (CW) signal with high gain and broad gain bandwidth with no need for time synchronization between the pump and the signal. In spite of the noncollinear arrangement of the amplifier, the spatial geometric smearing (SGS) is eliminated inside the amplifier due to the collinear Poynting vectors of the signal and the idler, which promotes the horizontal spatial resolution of the idler image to approach its vertical spatial resolution. Our experiments show that this design can improve the 2-D space–bandwidth product (SBP) of the idler imaging by a factor of 2.8, compared with the noncollinear type-I PM amplifier. The measured 2-D SBP is more than 73 000, which, to our knowledge, is the highest value for idler imaging to date.

Index Terms: Idler imaging, optical parametric amplification, spatial resolution, phase-matching.

1. Introduction

Optical parametric amplification (OPA) imaging has many advantages. For example, OPA can be used to carry out the wavelength-shift imaging with high gain [1] and the lensless phase conjugate imaging [2], [3]. Phase-sensitive noiseless OPA imaging [4], [5] can not only improve the signal-to-noise ratio, but also promote the angular resolution to approach Heisenberg limit [6]. The collinear degenerate OPA can simultaneously realize noncritical PM [7] for both the angle and the wavelength to optimize its spatial and spectral bandwidths. The pump intensity-dependent OPA gain and spatial/spectral bandwidths [8] provide a unique way to promote imaging quality. It is well known that using ultrashort laser pulses as the pump can offer the OPA imaging with high temporal resolution for ultrafast or time-resolved imaging [9], [10]. More interestingly, an optical parametric amplifiers pumped by ultrashort laser pulses can work at the pump intensities of up to several hundreds of GW/cm^2 [11], [12]. Consequently, the available OPA spectral bandwidth can be as wide as 250 THz [13], which implies that OPA is qualified

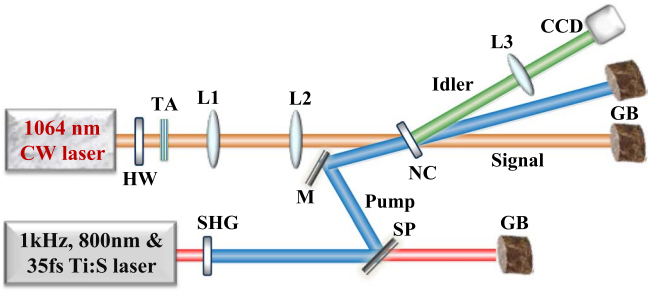

Fig. 1. Experimental setup for non-collinear OPA imaging. TA: Target object; L1~L3: Lenses; CCD: CCD camera; SHG: Second-harmonic generator; NC: Nonlinear optical crystal for OPA; HW: Half wave-plate; GB: Garbage bin; M: Mirror.

not only for the monochromatic imaging [14] but for the polychromatic imaging as well [15]. High pump intensity also provides large spatial bandwidth so the OPA pumped by ultrashort pulses can be used to implement signal imaging with a 2-D SBP of up to 46 000 [16]. What is more, high pump intensity means high OPA gain. Using intense ultrashort pulses as the pump allows an optical parametric amplifier to amplify effectively a CW signal from another separate laser source [17], which provides great flexibility to change the wavelength of the illuminating signal for OPA imaging. As a result, one can perform wavelength-shift imaging for different spectral demands or with a large tunable spectral region [18]. This paper presents a compact design for idler imaging. This design is based on type-II PM OPA pumped by an ultrashort pulse chain and seeded by a separate CW source. Despite the non-collinear arrangement, the Poynting vectors of the signal and the idler are collinear inside the nonlinear crystal, so the design can remove the SGS. Correspondingly, the horizontal spatial resolution of the idler image is improved by a factor of 2.24 compared with that in the type-I PM and is close to the vertical resolution. In our experiments, we have achieved an idler image with a 2-D SBP of greater than 73 000, which, to our knowledge, is the highest value for OPA idler imaging to date. Our calculations also show this design can implement idler imaging almost without SGS over a large spectral region.

2. Experimental Details

OPA imaging involves imaging a target with amplification and simultaneously generating a new beam (idler) with wavelength conversion and phase conjugation. As shown in Fig. 1, the signal beam used to illuminate a target (TA) is generated from a linearly-polarized CW laser operating at 1064 nm. The working power is set to be 1 W, although the maximal output power of the laser can be up to 10 W. A half wave-plate (HW) following the laser source is used to control the polarization of the CW beam. The signal diameter at $1/e^2$ intensity is expanded to about 10 mm in order to increase the illuminating area of the TA. A telescope including the lenses L1 and L2 images TA on to the front surface of a nonlinear crystal (NC) for OPA and reduces the beam size down to 5 mm to ensure effective pump. The pump laser is the second harmonic of a 1 kHz, 800 nm femtosecond pulse train from a commercial Ti:S laser system which can output a 35 fs linearly polarized pulse train with a pulse energy of up to 3 mJ. Using a wavelength separator (SP) coated with broadband anti-reflection centered at 800 nm and broadband high-reflection centered at 400 nm, the pump and the signal overlap each other with a small intersection angle (~2.46°) inside the nonlinear crystal (NC) for OPA. The NC is a β-BBO crystal that is used because of its large nonlinear coefficient and high laser damage threshold [19]. For a β-BBO OPA crystal, the pump acts as extraordinary ray for both type-I and type-II PM, whereas the signal acts as ordinary ray for type-I but can do as extraordinary ray for type-II PM. Accordingly, in order to switch between type-I to type-II PM OPA imaging, we need only replace the β-BBO crystal and rotate the signal polarization by the HW. The intensity of the pump (TEM_{00} mode) is estimated at 30 GW/cm^2, and the PM for OPA can be optimized by adjusting the crystal. The non-collinear arrangement makes us be able to select and record the idler images without need

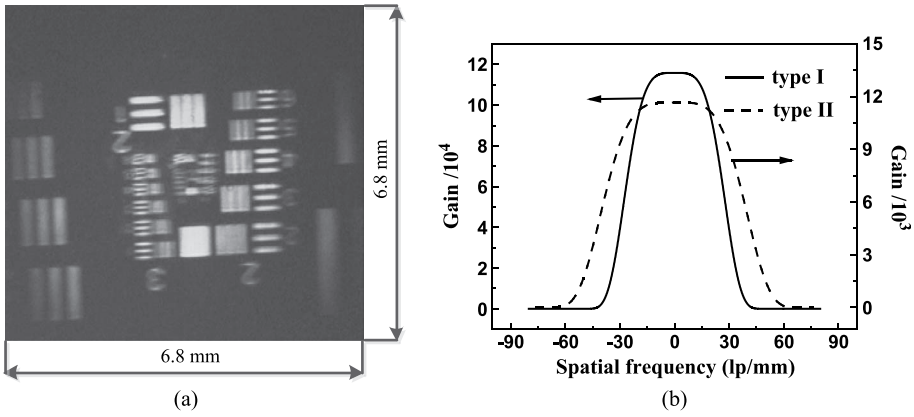

Fig. 2. (a) Idler image of the target USAF 1951(0) by use of a 29.2°-cut, 2 mm, type-I phase-matching β-BBO crystal and (b) the calculated parametric gain vs. spatial frequency using a 29.2°-cut, type-I (solid line) or 35.6°-cut, type-II (dotted line) non-collinear β-BBO optical parametric amplifiers seeded with CW 1064 nm laser and pumped by 400 nm ultrashort pulses.

of any wavelength separator and any polarization optics, which can lead to lose some polarization information of the idler images. As a result, we can conveniently implement optical imaging for different spectral demands. This alignment also allows the idler to be free from the disturbances of the pump and the signal due to the spatial separation among the three interactive waves. Because the β-BBO crystal is placed at the real image plane, so the idler images can be recorded by a CCD camera with 1280 $\times$ 960 pixels (CCD). A lens (L3) behind the CCD is used to image the front surface of the NC to the receiving surface of the CCD with 1$\times$ magnification. From above description, one can see that the OPA gain is independent of the input signal phase, so our setup performs phase-insensitive OPA imaging.

3. Results and Discussions

In our first experiment, we use a piece of 29.2°-cut, type-I PM β-BBO crystal with a thickness of 2 mm for idler imaging due to its high nonlinear conversion efficiency. The 400 nm pump has a pulse duration of ~30 fs, so the signal energy within this temporal scale can be estimated at 30 fJ. After OPA, the idler pulse energy is measured to be 1.75 nJ, much lower than the pump pulse energy (1 mJ). Theoretically, the spatial resolution of OPA imaging is mainly limited by the gain bandwidth and PM bandwidth, which depends on crystal length, pump intensity and PM condition [8]. The gain bandwidth increases and saturates to the PM bandwidth with the pump intensity [20] which is limited by the laser damage threshold of the nonlinear crystal and pump system. Here, we set the pump intensity at 30 GW/cm^2. In addition, gain bandwidth is proportional inversely to the crystal length, but a crystal that is excessively thin will sacrifice OPA gain. As a result, we choose the thickness to be 2 mm. The non-collinear angle is measured to be 2°. After aligning carefully the β-BBO crystal, we can get the idler around 641 nm with a bandwidth of about 8 nm. Using a USAF 1951(0) test pattern as target, we have recorded an idler image by a CCD camera as shown in Fig. 2(a). We find the image has the largest spatial features up to 20.16 lp/mm in the vertical and 8.98 lp/mm in the horizontal directions within an area of 6.8 mm $\times$ 6.8 mm. The vertical spatial resolution is lower slightly than the calculated gain bandwidth of 27.0 lp/mm as shown by the solid line in Fig. 2(b), which is reasonable because the gain bandwidth isn't the only one factor limiting the spatial resolution. However, the horizontal resolution is notably much lower than the vertical resolution thereby the calculated gain bandwidth.

Our analyses show the difference between the spatial resolutions in the vertical and horizontal directions may originate theoretically from SGS [21] and angular dispersion. The former arises when the β-BBO crystal is set in the real image plane as shown in Fig. 3(a). For the non-collinear type-I PM design, the spatial walk-off occurs among the interacting three-waves inside the OPA crystal. As a result, a point of image at the front surface of the crystal will evolve into a

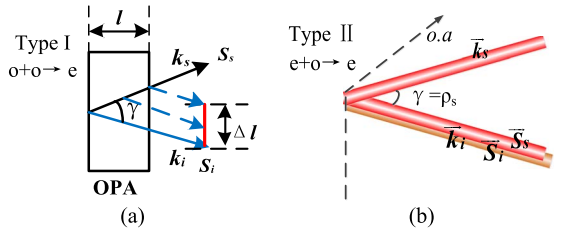

Fig. 3. (a) Spatial geometrical smearing arises in the non-collinear type-I PM OPA configuration and (b) the method to eliminate it in the non-collinear type-II PM OPA. o.a: optical axis.

line segment at the rear surface due to limited crystal thickness; this process degrades spatial resolution. The line segment length caused by SGS can be estimated by

$$\Delta l_{gs} \approx l \cdot \tan(\gamma) \tag{1}$$

where γ and l denote the crossing angle between the signal and the idler inside the crystal and the crystal thickness.

Because the pumping pulse train in our OPA imaging is broadband, the angular dispersion of the idler due to the non-collinear design may be another factor [22], [23] impairing the spatial resolution. The different wavelength components of a point on the front surface of the crystal will also become a line at the rear surface of the crystal in the idler image. The line length due to angular dispersion can be figured out by

$$\Delta l_{ad} \approx \left| l \times \tan\left[\Delta\lambda_i \cdot \frac{d\theta_i(\lambda_i)}{d\lambda_i}\right]\right|. \tag{2}$$

In (2), $\Delta\lambda_i$ is the spectral bandwidth while $d\theta_i(\lambda_i)/d\lambda_i$ is the angular dispersion of the idler where $\theta_i(\lambda_i)$ is the wavelength-dependent propagating angle of the idler inside the nonlinear crystal. According to (1) and (2), we get $\Delta l_{gs} \approx 110$ μm and $\Delta l_{ad} \approx 0.65$ μm in our setup. Obviously, the SGS effect on the OPA imaging is much stronger than the angular dispersion, so special attention shall be paid to the SGS rather than the angular dispersion. The line segment length $\Delta l_{gs} \approx 110$ μm caused by SGS means the largest visible spatial features in the horizontal direction of the idler images is about 9.1 lp/mm, very close to the measured value 8.98 lp/mm.

The conventional method to avoid SGS is to use a collinear OPA configuration when the image is placed in the real image plane. Fourier plane OPA imaging [16] is another way to prevent the imaging from SGS, where the image information is encoded by the propagating directions, rather than the spatial coordinates of the carrier waves [21]. However, the pump beam or the lateral dimension of the crystal acts as a low-pass filter, which means both the pump beam and the crystal are required to have large lateral sizes. Additionally, instead of SGS, Fourier plane OPA imaging will bring with spatial spectral geometric smearing; in other words, a point in the Fourier plane before OPA will become a line segment after OPA, which will distort the spatial spectrum thereby degrade the imaging quality.

In order to eliminate the SGS in a non-collinear OPA configuration, our basic idea is to design the nonlinear crystal to avoid the spatial walk-off between the signal and the idler inside the crystal. It is well known the direction of the wave vector is coincident with that of the Poynting vector for an ordinary ray, so it is impossible to remove the SGS in a non-collinear type-I PM β-BBO amplifier. In contrast, for an extraordinary ray, its Poynting vector deviates from its wave vector by a walk-off angle, which inspires us to remove the SGS by setting a proper non-collinear angle so that the crossing angle between the signal and the idler is equal to the walk-off angle between the Poynting vector and the wave vector of the signal. Fortunately, this idea can be realized in a type-II PM configure, where the idler beam acts as ordinary ray while the signal and the pump do as extraordinarily rays. As depicted in Fig. 3(b), the Poynting vector of signal deviates from the wave vector by a walk-off angle ρ_s but propagates in parallel with the Poynting vector of the idler

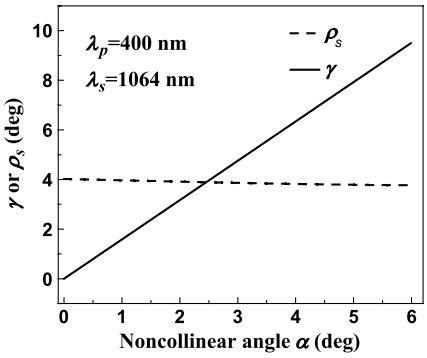

Fig. 4. Angle between signal and idler γ and the signal walk-off angle ρ_s versus non-collinear angle α in a type-II PM β-BBO crystal when $\lambda_s = 1064$ nm and $\lambda_p = 400$ nm.

which goes collinearly with the idler wave vector inside the β-BBO crystal, i.e., $\gamma = \rho_s$. Here we suppose the diameter of pump beam is large enough to avoid the deviations of the signal and the idler beams from the pump when propagating inside the NC.

It is well known that the PM condition in the non-collinear configuration can be expressed as

$$\begin{aligned} k_p &= k_s \cos\alpha + k_i \cos\beta \\ k_s \sin\alpha &= k_i \sin\beta \end{aligned} \tag{3}$$

where α and β are the angles between signal and pump and the angle between idler and pump, respectively, while $\gamma = \alpha + \beta$ refers to the crossing angle between signal and idler. The subscripts '*s*,' '*i*' and '*p*' represent the signal, idler and pump waves. The wave vector value $|k_j| = 2\pi n_j/\lambda_j$ ($j = s$, i, or p), n_j denotes the refractive index which depends on the polarization state and propagation direction of a ray inside the crystal, and λ_j denotes the wavelength of the signal, idler or pump. For a type-II PM uniaxial crystal (e.g., β-BBO) with the PM angles of $(\theta_s, \theta_i, \theta_p)$, if the signal acts as an extraordinary ray, its refractive n_s becomes θ-dependent, i.e.,

$$n_s(\theta_s) = n_o \sqrt{\frac{1 + \tan^2\theta_s}{1 + \left(\frac{n_o}{n_e}\right)^2 \tan^2\theta_s}} \tag{4}$$

where θ_s is the signal angle when (3) is met, and n_o or n_e represents the refractive index of the ordinary or extraordinary ray in principal plane. The walk-off angle ρ_s between the Poynting vector and the wave vector of the signal can be express by [24]

$$\rho_s(\theta) = \arctan\left(\frac{\sin(2\theta_s)}{2} \frac{n_o^2 - n_e^2}{n_o^2 \sin^2\theta_s + n_e^2 \cos^2\theta_s}\right). \tag{5}$$

Accordingly, if $\gamma = \rho_s$, (5) becomes

$$\alpha + \beta = \arctan\left(\frac{\sin(2\theta_s)}{2} \frac{n_o^2 - n_e^2}{n_o^2 \sin^2\theta_s + n_e^2 \cos^2\theta_s}\right). \tag{6}$$

From (3)–(6), we can figure out both α, β and θ_s. Fig. 4 shows our numerical calculations on the angle between signal and idler γ and the signal walk-off angle ρ_s versus non-collinear angle α in a type-II PM β-BBO amplifier. One can see that $\gamma = \rho_s$ occurs at $\alpha = 2.46°$ where the Poynting vectors of signal and idler are collinear inside a 35.6°-cut β-BBO crystal.

According to Fig. 4, we have designed a 2 mm-thick, 35.6°-cut, type-II PM β-BBO crystal with a non-collinear angle of 2.46° to remove the SGS. When $\lambda_s = 1064$ nm and $\lambda_p = 400$ nm, Fig. 2(b) presents the parametric gain of this design vs. spatial frequency with the dotted line under a

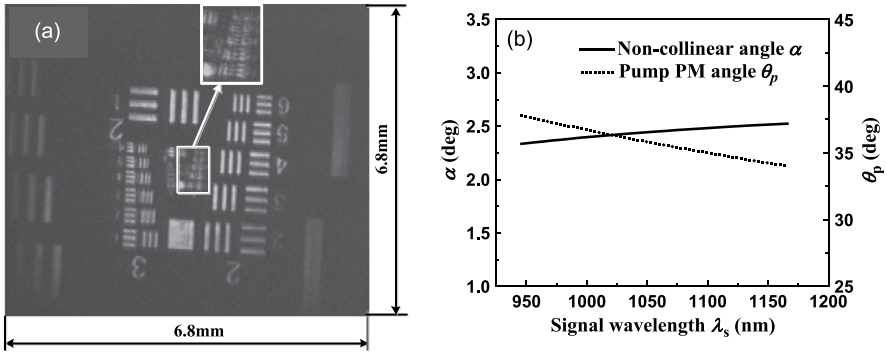

Fig. 5. (a) Measured idler image of the target USAF 1951(0) and (b) the calculated non-collinear angle α and the pump PM angle θ_p vs. signal wavelength by use of a 2 mm-thick, 35.6°-cut and type-II PM β-BBO crystal as optical parametric amplifier pumped by 400 nm ultrashort laser pulses.

pump intensity of 30 GW/cm^2. The calculated 3 dB bandwidth is 38 lp/mm, which is larger than 27 lp/mm: that in the type-I case (the solid line).

After rotating the HW in Fig. 1 so that the polarization of the CW 1064 nm laser is parallel to that of the 400 nm pump, we can begin our second experiment, the type-II PM OPA imaging, just by using a 35.6°-cut 2 mm-thick type-II PM β-BBO crystal to replace the 29.2°-cut type-I PM one. The idler pulse energy is measured to be 0.23 nJ with corresponding parametric gain up to 1.2×10^4. Fig. 5(a) is the recorded idler image of the target USAF 1951(0) with the type-II non-collinear optical parametric amplifier. The image has the largest spatial features up to 20.16 lp/mm in the horizontal direction and 25.39 lp/mm in the vertical direction, with an area of 6.8 mm $\times$ 6.8 mm. Compared with the idler image shown in Fig. 2(a), Fig. 5(a) shows the type-II PM design has improved the spatial resolutions in both the horizontal and the vertical directions, which agrees with the theoretical results in Fig. 2(b). In Fig. 2(b), the pump depletion can be neglected because the pulse energy of the amplified idler is much smaller than the pump pulse energy. Especially in the horizontal direction, the measured spatial resolution has increased by more than 2.24 times, which verifies our preceding analyses by (1) and (2). The removal of the SGS allows the idler imaging to have its horizontal spatial resolution close to its vertical resolution. However, the measured resolutions in both directions are still lower slightly than the calculated values in Fig. 2(b), which is understandable because the gain bandwidth is not the only factor restricting the spatial resolutions of OPA imaging. In addition, the horizontal resolution is still lower than the vertical. Besides the phase-mismatching among the interactive three waves and the angular dispersion of the broadband idler, we think the rest SGS still plays role in blurring the idler images because our type-II PM design can actually eliminate the SGS caused from the information carried by the low spatial frequencies. Nevertheless, Fig. 5(a) shows we have get an idler image with a 2-D SBP more than 73000.

In Fig. 5(b), we calculate the non-collinear angle α and the pump PM angle θ_p vs. signal wavelengths λ_s around 1064 nm when keeping $\rho_s = \gamma$ in our type-II PM configuration pumped by 400 nm ultrashort laser pulses. The angle α increases from 2.34° to 2.52°, whereas θ_p decreases from 37.8° to 34.0° with the signal wavelength from 946 nm to 1166 nm. The calculated spatial bandwidth changes from 33.6 lp/mm to 38.8 lp/mm. The insensitivities of α and θ to λ_s mean that, although our setup is design for a signal wavelength of 1064 nm, it can also work for a wide spectral region ranging from 946 nm to 1166 nm to realize high spatially-resolved idler imaging only by subtly tuning the direction of the crystal and the incidence angles of the signal.

4. Conclusion

This paper reports a high spatially-resolved non-collinear OPA idler imaging with a 2-D SBP greater than 73000 and a parametric gain of up to 10^4, where the signal is a CW laser beam. Besides the intense femtosecond pulse laser pump, the high 2-D SBP shall be attributed mainly to

the removal of SGS by choosing a non-collinear type-II PM configuration. According to our experiments, the recorded idler image has the largest spatial features up to 20.16 lp/mm in the horizontal and 25.39 lp/mm in the vertical directions within an imaging area of 6.8 mm $\times$ 6.8 mm. According to our calculations, this non-collinear type-II PM configuration can ensure to remove the SGS over a large spectral region. Our setup uses a CW laser as signal, which can avoid the complicated temporal synchronization between the signal and pump, thereby simplify the setup. The non-collinear arrangement needs no polarization optics or wavelength separator to select and record the idler images, which cannot only abate the loss of the idler image information and be free from the disturbances of the pump and the signal but implement conveniently optical imaging for different spectral demands as well. In conclusion, we have presented a compact setup, which can implement idler imaging with large 2-D SBP over a large spectral region.

References

[1] E. Lantz and F. Devaux, "Parametric amplification of images," *J. Opt. B, Quantum Semiclassical Opt.*, vol. 9, no. 2, pp. 279–286, Apr. 1997.

[2] F. Devaux, G. Le Tolguenec, and E. Lantz, "Phase conjugate imaging by type II parametric amplification," *Opt. Commun.*, vol. 147, no. 4–6, pp. 309–312, Feb. 1998.

[3] L. Lefort and A. Barthelemy, "Image restoration through aberrant media by optical phase conjugation in a type II three-wave mixing interaction," *Opt. Lett.*, vol. 23, no. 20, pp. 1597–1599, Oct. 1998.

[4] S.-K. Choi, M. Vasilyev, and P. Kumar, "Noiseless optical amplification of images," *Phys. Rev. Lett.*, vol. 83, no. 10, pp. 1938–1941, Sep. 1999.

[5] A. Mosset, F. Devaux, and E. Lantz, "Spatially noiseless optical amplification of images," *Phys. Rev. Lett.*, vol. 94, no. 22, Jun. 2005, Art. ID 223603.

[6] Z. Huang, D. French, H. Y. Pao, and I. Jovanovic, "Assessment of image resolution improvement by phase-sensitive optical parametric amplification," *Appl. Phys. B.*, vol. 102, no. 3, pp. 607–613, Mar. 2011.

[7] E. Lantz, L. Han, and A. Laciurt, "Simultaneous angle and wavelength one-beam noncritical phase matching in optical parametric amplification," *Opt. Commun.*, vol. 97, no. 3/4, pp. 245–249, Mar. 1993.

[8] M. Vasilyev, N. Stelmakh, and P. Kumar, "Estimation of the spatial bandwidth of an optical parametric amplifier with plane-wave pump," *J. Mod. Opt.*, vol. 56, no. 18/19, pp. 2029–2033, Oct. 2009.

[9] Q. Ding, K. Meng, H. Yang, S. Wang, and Q. Gong, "Femtosecond noncollinear parametric amplification for ultrafast spectral dynamics," *Opt. Commun.*, vol. 284, no. 12, pp. 3110–3113, Jun. 2011.

[10] G. Le Tolguenec, F. Devaux, and E. Lantz, "Two-dimensional time-resolved direct imaging through thick biological tissues: A new step toward noninvasive medical imaging," *Opt. Lett.*, vol. 24, no. 15, pp. 1047–1049, Aug. 1999.

[11] J. Rothhardt, S. Demmler, S. Hädrich, J. Limpert, and A. Tünnermann, "Octave-spanning OPCPA system delivering CEP-stable few-cycle pulses and 22 W of average power at 1 MHz repetition rate," *Opt. Exp.*, vol. 20, no. 10, pp. 10870–10878, May 2012.

[12] P. S. Banks, M. D. Feit, and M. D. Perry, "High-intensity third-harmonic generation," *J. Opt. Soc. Amer. B, Opt. Phys.*, vol. 19, no. 1, pp. 102–108, Jan. 2002.

[13] T. Kobayashi and A. Baltuska, "Sub-5 fs pulse generation from a noncollinear optical parametric amplifier," *Meas. Sci. Technol.*, vol. 13, no. 11, pp. 1671–1682, Oct. 2002.

[14] F. Devaux *et al.,* "Picosecond parametric amplification of a monochromatic image," *Nonlinear Opt.*, vol. 11, pp. 25–37, Jun. 1995.

[15] F. Devaux and E. Lantz, "Parametric amplification of a polychromatic image," *J. Opt. Soc. Amer. B, Opt. Image Sci.*, vol. 12, no. 11, pp. 2245–2252, Nov. 1995.

[16] P. M. Vaughan and R. Trebino, "Optical-parametric-amplification imaging of complex objects," *Opt. Exp.*, vol. 19, no. 9, pp. 8920–8929, Apr. 2011.

[17] X. Zeng *et al.,* "High gain and high spatial resolution optical parametric amplification imaging under continuous-wave laser irradiation," *Laser. Phys.*, vol. 24, no. 4, Mar. 2014, Art. ID 045401.

[18] J. Storteboom *et al.,* "Incoherently pumped continuous wave optical parametric oscillator broadened by non-collinear phase matching," *Opt. Exp.*, vol. 19, no. 22, pp. 21786–21792, Oct. 2011.

[19] M. Ghotbi, M. Ebrahim-Zadeh, A. Majchrowski, E. Michalski, and I. V. Kityk, "High-average-power femtosecond pulse generation in the blue using BiB_3O_6," *Opt. Lett.*, vol. 29, no. 21, pp. 2530–2532, Nov. 2004.

[20] L. Hongjun *et al.,* "Investigation of spectral bandwidth of optical parametric amplification," *Appl. Phys. B*, vol. 79, no. 5, pp. 569–576, Sep. 2004.

[21] R. A. Andrews, "IR image parametric up-conversion," *IEEE J. Quantum Electron.*, vol. QE-6, no. 1, pp. 68–80, Jan. 1970.

[22] S.-W. Huang, J. Moses, and F. X. Kartner, "Broadband noncollinear optical parametric amplification without angularly dispersed idler," *Opt. Lett.*, vol. 37, no. 14, pp. 2796–2798, Jul. 2012.

[23] R. Ye, B. Zhang, and N.-C. Sun, "SNR improvement based on non-collinear OPCPA with angular spectral dispersion in BBO crystal," *Opt. Commun.*, vol. 322, pp. 27–31, Jul. 2014.

[24] V. G. Dmitriev, G. G. Gurzadyan, and D. N. Nikogosyan, *Handbook of Nonlinear Optical Crystals*. Berlin, Germany: Springer-Verlag, 2008.